Supporting Information

Signal Transduction in Human Cell Lysate via Dynamic RNA Nanotechnology

Lisa M. Hochrein,[1] Tianjia J. Ge,[1] Maayan Schwarzkopf[1] and Niles A. Pierce[1,2,3]

Contents

[1]Division of Biology & Biological Engineering, California Institute of Technology, Pasadena, CA 91125, USA. [2]Division of Engineering & Applied Science, California Institute of Technology, Pasadena, CA 91125, USA. [3]Weatherall Institute of Molecular Medicine, University of Oxford, Oxford OX3 9DS, UK. *Email: niles@caltech.edu

List of Figures

List of Tables

S1 Methods

S1.1 Computational sequence design and analysis

scRNA sequences were designed using the reaction pathway engineering tools within NUPACK (`nupack.org`).[2,3] Within each target test tube in the design ensemble, all on-target complexes had a target concentration of 2.5 nM and all off-target complexes (consisting of all complexes of up to 4 strands) had a target concentration of 0 nM. Target test tubes displaying target structures for on-target complexes are shown for the forward system ($X \dashv Y$) in Figure 2a and for the reverse system in ($Y \dashv X$) in Figure S1a. In these panels, nucleotides are shaded to depict sequence constraints imposed by mRNAs X (magenta shading) and Y (green shading). For the forward mechanism, the design algorithm selected an scRNA binding site from within the full-length mRNA X sequence. For the reverse mechanism, we used RNAhyb to experimentally identify an accessible window of the full-length mRNA Y, from which the designer selected an scRNA binding site. For a given design, the sequences were optimized by mutating the sequence set to reduce the multi-tube ensemble defect.[3] Designs were performed using RNA parameters for 37°C in 1M Na^+.[4] Chemical modifications (2′OMe-RNA) used to reduce RNase-mediated degradation and Mg^{++} (in buffer D) used to facilitate Dicer processing were not accounted for in the physical model.

For the final sequence designs, equilibrium analysis of the target test tubes reveals the contributions of structural defects (fraction of nucleotides in the incorrect base-pairing state within the ensemble of an on-target complex) and concentration defects (fraction of nucleotides in the incorrect base-pairing state because there is a deficiency in the concentration of an on-target complex) to the overall multi-tube ensemble defect. Residual defects are displayed in Figure 2b for the forward system and in Figure S1b for the reverse system. In these panels, tubes depict the predicted concentration and target structure for each on-target complex, with nucleotides shaded to indicate the probability of adopting the depicted base-pairing state at equilibrium (nucleotides shaded dark red adopt the depicted state with probability close to 1 and contribute negligible structural defect; nucleotides shaded dark blue adopt the depicted state with probability close to 0 and contribute maximal structural defect). Bar graphs depict the residual defect for each on-target complex in each tube.

It is interesting to note that when analyzed in isolation, the short RNA input X_s for the forward mechanism is predicted to be relatively unstructured (Figure S2a), while the short RNA input Y_s for the reverse mechanism is predicted to be highly structured (Figure S2b) even though RNAhyb experimental data established that this subsequence is relatively accessible in the context of the full-length mRNA Y. The short RNA input was not included in the Reactants tube due to the unreliability of predictions for this short subsequence in isolation from the full-length mRNA.

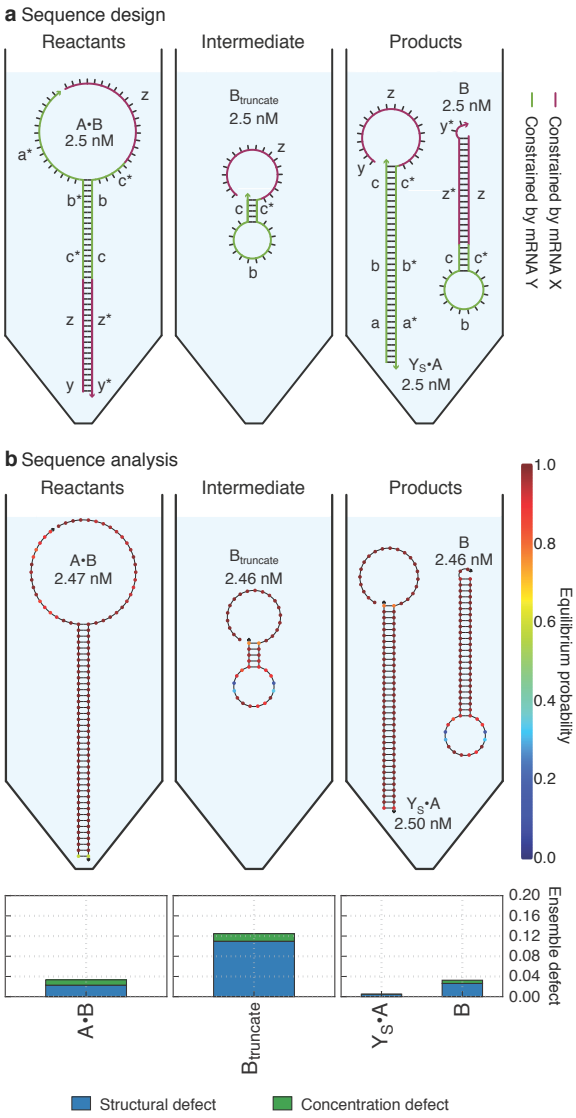

Figure S1: scRNA sequence design and analysis for the reverse molecular logic Y ⊣ X. (a) Target test tubes depicting the target structure and target concentration for each on-target complex, with nucleotides shaded to depict sequence constraints imposed by mRNA input Y (green nucleotides) or mRNA silencing target X (magenta nucleotides). In each tube, off-targets include all complexes of up to 4 strands (not depicted). (b) Analysis of design quality over the design ensemble. Tubes depict the predicted concentration and target structure for each on-target complex, with nucleotides shaded to indicate the probability of adopting the depicted base-pairing state at equilibrium. In the Reactants tube, the scRNA reactant A·B is predicted to be well-formed with an accessible toehold 'a*'. In the Intermediate tube, the internal toehold 'c' is predicted to nucleate with complement 'c*' with high probability, and there is some unwanted secondary structure in the hairpin loop. In the Products tube, the waste duplex Y_S·A and the shRNA Dicer substrate B are both predicted to be well-formed (again with unwanted secondary structure in the loop of B). On-target complexes that form at concentrations below the 2.5 nM target concentration indicate the formation of off-target complexes at non-negligible concentrations. Bar graphs depict the residual defect for each on-target complex in each tube. For all three tubes, the concentration defect is smaller than the structural defect. RNA at 37 °C in 1 M Na^+.

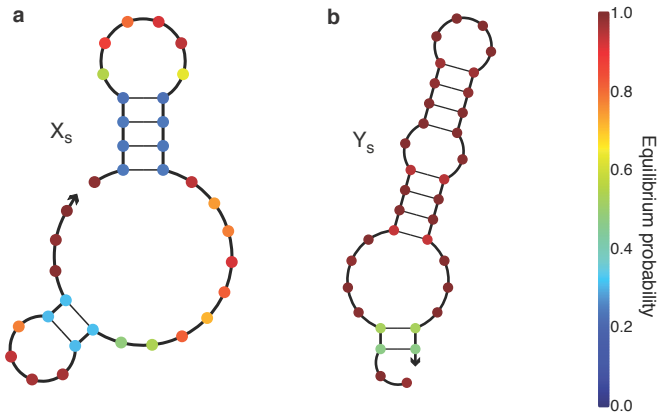

Figure S2: Predicted minimum free energy structure of short RNA inputs analyzed in isolation from the remainder of the full-length mRNA. (a) Short RNA input X_s for the forward logic X ⊣ Y. (b) Short RNA input Y_s for the reverse logic Y ⊣ X. Nucleotide shading indicates the probability of adopting the depicted base-pairing state at equilibrium. RNA at 37 °C in 1 M Na^+.

S1.2 Oligonucleotide synthesis and radioactive labeling

Oligonucleotides (RNA and modified RNA) were chemically synthesized and RNase-free HPLC purified by Integrated DNA Technologies (IDT). Strand B was labeled with ^{32}P in order to distinguish scRNA A·B, shRNA B, and the resulting siRNA from lysate-derived nucleic acids. After observing that 5′-^{32}P was efficiently removed in lysate (thus eliminating our ability to image the gel), we devised a method to internally label B, which forms a hairpin in isolation from A. The hairpin was synthesized in two pieces: B_1 and B_2. The location of the strand break was chosen to be contained within the final siRNA so that the ^{32}P would be present in the final siRNA output. B_2 was 5′-^{32}P labeled. 50 μL 5′-^{32}P labeling reactions of short 3′ fragment (B_2, 2 μM) or siRNA markers (NEB, N2101, 5 μL) used T4 Polynucleotide Kinase (NEB, M0201) and a limiting amount of ATP. Non-radioactive ATP (NEB, P0756) was used in combination with [γ-^{32}P] ATP (10 mCi/mL, 3000 Ci/mmol, PerkinElmer, BLU002A250UC) to ensure that the reactions contained 1 μM ATP with 10% [γ-^{32}P] ATP. Unincorporated ATP was removed using illustra MicroSpin G-25 columns (GE Healthcare, 27-5325-01) according to manufacturer instructions. Radioactive signal counts per minute (CPM) were measured on a Beckman liquid scintillation counter (LS 6000SC). 5′-^{32}P labeled B_2 (39 pmol) was annealed (90 °C for 3m, cool to 23 °C at 1 °C/m, hold 23 °C) to a limiting amount of B_1 (25 pmol) to form a hairpin structure with a nick in the stem (49 μL reaction, 1× RNA ligase 2 buffer). Ligation with 10 units T4 RNA Ligase 2 (NEB, M0239) resulted in a hairpin that contained ^{32}P within the RNA backbone located approximately in the middle of the hairpin stem. The labeled hairpin was purified by spin column chromatography (Oligo Clean & Concentrator, Zymo, D4060). The scRNA duplex A·B was prepared by annealing ^{32}P-labeled B to an excess of A (20 μL reaction: 1× Buffer D-, 17 pmol B, 25 pmol A), separating via native PAGE (12% native TBE polyacrylamide gel, 200 V for 3 h at room temperature in 1× TBE) and excising the A·B band. The scRNA duplex was eluted from the excised gel piece by crushing with a Squisher (Zymo Research, H1001) in 1× Buffer D– (20 mM HEPES, pH 7.5; 100 mM KCl; 0.2 mM EDTA, pH 8.0; 5% glycerol) followed by an incubation at 4 °C overnight (or longer). The supernatant was filtered through a Nanosep MF Centrifugal Device, 0.45 μm (Pall, ODM45C34) at 10,000 g for 3 min and stored at 4 °C to help retain the correct secondary structure.

S1.3 Cell lysate preparation

Human cell lysate was generated by sonication of HEK 293T cells following the method of Sakurai et al.[5] Briefly, HEK 293T (ATCC, CRL-3216) cells were grown to confluency in 10 cm dishes, trypsinized, harvested, and washed with DPBS. The pelleted cells were re-supsended in 0.5 mL of 1× Buffer D (20 mM HEPES, pH 7.5; 100 mM KCl; 0.2 mM EDTA, pH 8.0; 5% glycerol; 0.5 mM DTT; 1× HALT^{TM} Protease Inhibitor Cocktail, EDTA-free (Thermo Fisher Scientific, 78425)) per 10 cm plate of cells. The suspended cells were lysed in either 2 mL or 5 mL Eppendorf tubes depending on volume to be lysed. A Misonix S-4000 sonicator with a 2 mm microtip delivered six 10 s 20% amplitude pulses with 30 s breaks. The cells were kept on ice or in a chilled metal block to prevent overheating. The lysate was cleared by centrifugation at 13,000 g for 15 min at 4 °C and either immediately flash frozen (wildtype lysate) or immunodepleted (Dicer-depleted lysate and control lysate) and then flash frozen. The lysate was aliquoted for single use, frozen in a dry ice/ethanol bath, and stored at –80 °C. Lysate total protein concentration, used to normalize lysate per reaction, was determined in triplicate with a Pierce BCA Protein Assay kit (Thermo Fisher Scientific, 23225) using a BSA standard by measuring A562 on a plate reader (BioTek Synergy Neo2 or equivalent). Lysate total protein concentration was in the range of 3–5 mg/mL. For Dicer-depleted lysate, Dicer was removed from the lysate via a two-step process: siRNA silencing of Dicer prior to lysis followed by Dicer immunodepletion after lysis. Three

days prior to lysis, the HEK 293T cells were transfected with 20 nM Dicer siRNA (Santa Cruz Biotechnology, sc-40489) using Lipofectamine RNAiMAX (Thermo Fisher Scientific, 13778030). The cells were lysed as described above and immunodepled using an anti-Dicer antibody following a protocol modified from Sakurai et al.[5] Briefly, immunodepletion consisted of gently rotating 20 μg anti-Dicer antibody (abcam, ab14601) per 1 mL lysate overnight at 4 °C on a rotisserie rotator. 300 μL Protein G agarose beads, high affinity (abcam, ab193258) per 1 mL lysate were washed three times in 1× Buffer D, resuspended in 1× Buffer D and added to the lysate. The beads and lysate were incubated for 6 h at 4 °C with gentle rotation. The beads were removed by centrifugation at 1000 g for 5 min at 4 °C. The resulting Dicer-depleted lysate was flash frozen as described above. Control lysate followed the same protocol except that the Dicer siRNA and anti-Dicer antibody were replaced with an equivalent amount of buffer.

S1.4 Concentration estimates for cells and lysate

To estimate the needed siRNA concentration in vivo, note that Pei et al. measured knockdown of the target gene *Ssb* varying from 50%–87% for 370–2200 copies of the siRNA guide strand per mouse liver cell.[6] Most mammalian cells have a volume in the range of 0.5–4 pL/cell.[7] The lower and upper bounds on molar concentration are then estimated as:

$$c_{\text{lower}} = \frac{370 \text{ molecules/cell}}{6.02 \times 10^{23} \text{ molecules/mol} \cdot 4 \times 10^{-12} \text{ L/cell}} = 0.15 \text{ nM},$$

$$c_{\text{upper}} = \frac{2200 \text{ molecules/cell}}{6.02 \times 10^{23} \text{ molecules/mol} \cdot 0.5 \times 10^{-12} \text{ L/cell}} = 7 \text{ nM},$$

corresponding to an siRNA concentration range of 0.15–7 nM for effective silencing.

To estimate the dilution factor from cells to lysate, note that our scRNA signal transduction experiments were performed in lysate containing 1.25 μg of total protein per μL. During lysate preparation, we estimate that 5000 cells are lysed to produce 1 μg of total protein. Hence, for a cellular volume of 0.5–4 pL/cell,[7] lower and upper bounds on the dilution factor are:

$$d_{\text{lower}} = \frac{1 \ \mu\text{g}}{5000 \text{ cell} \cdot 4 \times 10^{-12} \text{ L/cell} \cdot 1.25 \times 10^{6} \ \mu\text{g/L}} = 40,$$

$$d_{\text{upper}} = \frac{1 \ \mu\text{g}}{5000 \text{ cell} \cdot 0.5 \times 10^{-12} \text{ L/cell} \cdot 1.25 \times 10^{6} \ \mu\text{g/L}} = 320,$$

corresponding to a dilution factor of 40–320 moving from cells to lysate. Alternatively, Gillen and Forbush measured 154 μg total protein per μL in HEK293 cells,[8] yielding a dilution estimate of

$$d_{\text{alternate}} = \frac{154 \ \mu\text{g}/\mu\text{L}}{1.25 \ \mu\text{g}/\mu\text{L}} = 123 \tag{S1}$$

consistent with the lower and upper bounds above.

S1.5 mRNA in vitro transcription

5′-capped, 3′-polyadenylated mRNA was created through in vitro transcription, capping, and tailing using CellScript's T7 mScript Standard mRNA Production System (C-MSC11610). DsRed2 and d2EGFP mRNA sequences matching those found in our HEK293 d2EGFP + DsRed2 cell line were cloned into the pTnT vector (Promega, L5610) via Gibson assembly (NEB, E2611). The appropriate plasmid was linearized with Spe1-HF (NEB, R3133) and used as a template in the mRNA production system. The mRNA mass concentration (ng/μL) was determine via A260 measurements on a NanoDrop 8000 Spectrophotometer (Thermo Fisher Scientific, ND-8000) assuming 1 OD at 260 nM = 40 ng/μL. Mass concentration was converted to molar concentration via the following molecular weights: DsRed2 mRNA = 345,036 g/mol, d2EGFP mRNA = 387,342 g/mol. These molecular weights are approximate due to variation in the length of the poly(A) tail.

S1.6 scRNA signal transduction reactions

The concentration of 5′-^{32}P labeled B_2 was calculated based on the assumption that all the ATP in the labeling reaction is consumed. This concentration can then be used to approximate scRNA concentrations by using the ratio of scRNA radioactive signal (CPM) to the corresponding 5′-^{32}P labeled B_2 radioactive signal. Unlabeled strand concentrations were calculated using NanoDrop 8000 Spectrophotometer A260 measurements and extinction coefficients provided by IDT. Immediately prior to signal transduction reactions:

1. scRNA A·B was diluted from stock stored at 4 °C to 20 nM in 1× Buffer D–,
2. mRNA was diluted to 100 nM in 1× Buffer D– and relaxed (65 °C for 5 min; room temperature for ≥30 min),
3. shRNA B (to serve as a control) was snap cooled (95 °C at 90 s; ice for 30 s; room temperature for ≥30 min) at 20 nM in 1× Buffer D–,
4. mRNA complexed with blocker strand L (to serve as a control) was prepared by heating a mixture containing 400 nM blocker and 100 nM mRNA in 1× Buffer D– to 65 °C for 5 min, followed by room temperature for ≥30 min.

Signal transduction reactions were performed in 20 μL containing 25 μg cell lysate, 2.5 nM scRNA (scRNA A·B or shRNA B), and 10 nM RNA input (either full-length mRNA, short RNA, or mRNA complexed with blocker) in 1× Buffer D. Final concentration 6.4 mM $MgCl_2$ (Ambion, AM9530G), necessary for Dicer cleavage, and 1× HALT^{TM} protease inhibitor were added to all reactions. Reactions were incubated at 37 °C for 4 h except for the gels in Figures S4, S5, S6, S12, and S13, which were incubated for 2 h. Most reactions were immediately separated by native PAGE. For the reactions in Figures S4, S5, and S6, the lysate proteins were removed before separation by native PAGE. Protein removal consisted of protein degradation by adding 1 μL (∼20 μg) Proteinase K (NEB, P8107S) and 29 μL PK buffer (200 mM Tris-HCl, pH 7.5; 25 mM EDTA; 300 mM NaCl; 2% wt/vol sodium dodecyl sulfate)[9] and incubating at 37 °C for 30 min. The nucleic acids were then purified using an Oligo Clean & Concentrator kit (Zymo, D4060) and eluted in 20 μL water (10 μL water for the reactions in Figure S5).

S1.7 Native polyacrylamide gel electrophoresis

The reactions were analyzed by native PAGE using 20% TBE polyacrylamide gels run at 200 V for 8 h at room temperature in 1× TBE. Samples were mixed with 5× native loading dyes and the gel wells were loaded with 2,000 – 10,000 CPM (adjusted sample volume to ensure a constant CPM per lane across the gel). Every other lane was skipped to prevent crosstalk between lanes. Gels were exposed for approximately 24 h to a storage phosphor screen (BAS-IP) and imaged using the IP-S settings of the FujiFilm FLA-5100 imaging system.

S1.8 Gel quantification

Quantification was performed using Multi Gauge software (FujiFilm). To calculate the ON:OFF ratio, we quantify siRNA production in the presence of either the cognate mRNA input (ON state) or a non-cognate mRNA input (OFF state). For a given lane containing reaction products, we calculate the mean intensity, representing a combination of signal and background, for each of two boxes: (1) siRNA bands box and (2) full lane box. The background component is then estimated using boxes equivalently positioned within the empty lanes on either side. siRNA production was calculated as the ratio of background-subtracted signal in the siRNA box divided by the background-subtracted signal in the full lane box. Let $\bar{x}_{\mathrm{ON}}$ and s_{ON} denote the sample mean and standard error for the ON state over three replicate lanes, and let $\bar{x}_{\mathrm{OFF}}$ and s_{OFF} denote the sample mean and standard error for the OFF state over three replicate lanes. The ON/OFF ratio is then estimated as

$$\bar{x}_{\mathrm{ON/OFF}} = \bar{x}_{\mathrm{ON}} / \bar{x}_{\mathrm{OFF}}$$

with standard error estimated via uncertainty propagation as

$$s_{\mathrm{ON/OFF}} \leq \frac{\bar{x}_{\mathrm{ON}}}{\bar{x}_{\mathrm{OFF}}} \sqrt{\left(\frac{s_{\mathrm{ON}}}{\bar{x}_{\mathrm{ON}}}\right)^2 + \left(\frac{s_{\mathrm{OFF}}}{\bar{x}_{\mathrm{OFF}}}\right)^2}.$$

This upper bound on estimated standard error holds under the assumption that the correlation between ON and OFF is non-negative.

S1.9 RNAhyb

We followed the protocol of Section S2 to measure the accessibility of in vitro transcribed d2EGFP mRNA (input mRNA Y for the reverse mechanism) using 20-nt DNA probes. Initially, we tested probes complementary to the mRNA at 10-nt intervals. Additional probes were tested in regions of interest (see Table S4 for a complete list of probes).

S2 RNAhyb protocol

The RNAhyb assay enables direct experimental measurement of the accessibility of different windows along an mRNA.

- **Step 1. Unpurified DNA probes:** Order unpurified short DNA probes (default: 20 nt) complementary to subsequences along the mRNA at regular intervals (default: 10 nt).
- **Step 2. Radioative labeling:** Label each DNA probe with 5′-^{32}P by incubating 100 pmol probe with 20 units T4 Polynucleotide Kinase (NEB, M0201) and 0.2-0.5 μL end-labeling grade ATP γ-^{32}P (MP Biomedicals, 013502002) in a 50 μL reaction volume at 37 °C for 1 h. Heat inactive T4 Polynucleotide Kinase by heating to 65 °C for 20 m. Remove unincorporated ATP using an illustra MicroSpin G-25 column (GE Healthcare, 27-5325-01).
- **Step 3. Hybridization:** Incubate 2.5 nM probes with 10 nM mRNA (stock concentrations determined by A260 measurements on a NanoDrop and converted to molar units using the appropriate extinction coefficient) for 2 h at 37 °C in 1× Buffer D– supplemented with 6.4 mM $MgCl_2$ and 1× HALT protease inhibitor.
- **Step 4. Native PAGE and autoradiography:** Run a 4–20% native gel (BioRad, 4565056), expose to a storage phosphor screen (BAS-IP) for approximately 24 h and image with the IP-S settings of an imagining system (e.g., FujiFilm FLA-5100). Example gels are shown in Figures S12 and S13.
- **Step 5. Quantification:** Quantify the band representing the mRNA:probe complex and normalize the signal relative to the total lane signal after background subtraction. Example hybridization yields are shown in Figure S11.

Figure S3 illustrates mRNA:probe hybridization and the expected appearance of the gel bands.

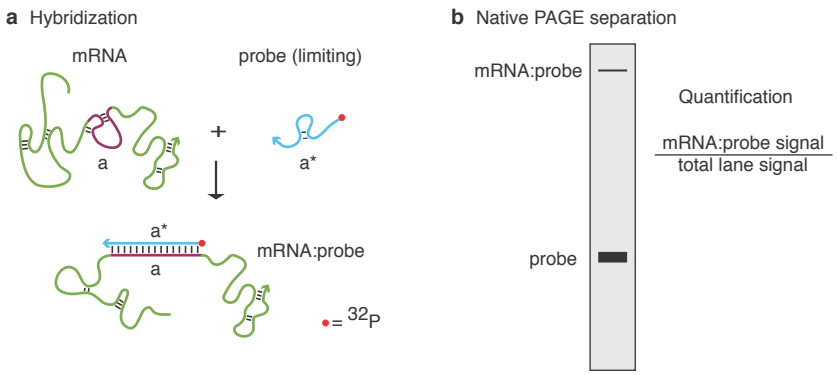

Figure S3: RNAhyb protocol schematic. (a) Hybridization: the mRNA of interest and a limiting amount of probe are incubated together in the relevant conditions. A separate hybridization reaction is performed for each probe. (b) Native PAGE separation: Separation of the bound versus unbound probe by native PAGE followed by autoradiography allows for quantification of the mRNA:probe binding.

S3 Sequences

S3.1 scRNA sequences for forward mechanism (X ⊣ Y) and reverse mechanism (Y ⊣ X)

a Forward mechanism sequences (X ⊣ Y)

Strand	Domains	Sequence
X_S	a-b-c	5′–CAGCUUAUAAUGGUUACAAAUAAAGCAAUAGCAUC–3′
A	y-z-c*-b*-a*	5′–ACUUCAAGAUCCGCCACAACAGAUGCUAUUGCUUUAUUUGUAACCAUUAUAAGCUG–3′
B	z-c*-b-c-z*-y*	5′–UUCAAGAUCCGCCACAACAGAUGCCAAAUAAAGCAAUAGCAUCUGUUGUGGC^{32P}GGAUCUUGAAGU–3′
B_1		5′–UUCAAGAUCCGCCACAACAGAUGCCAAAUAAAGCAAUAGCAUCUGUUGUGGC–3′
B_2		5′–GGAUCUUGAAGU–3′
L_X	3nt-a*-3nt	5′–UUGUAACCAUUAUAAGCUGCAA–3′

b Reverse mechanism sequences (Y ⊣ X)

Strand	Domains	Sequence
Y_S	a-b-c	5′–CAACGAGAAGCGCGAUCACAUGGUCCUGCUGGAGU–3′
A	y-z-c*-b*-a*	5′–AGCAUCACAAAUUUCACAAAUACUCCAGCAGGACCAUGUGAUCGCGCUUCUCGUUG–3′
B	z-c*-b-c-z*-y*	5′–CAUCACAAAUUUCACAAAUACUCCCACAUGGUCCUGCUGGAGUAUUUGU^{32P}GAAAUUUGUGAUGCU–3′
B_1		5′–CAUCACAAAUUUCACAAAUACUCCCACAUGGUCCUGCUGGAGUAUUUGU–3′
B_2		5′–GAAAUUUGUGAUGCU–3′
L_Y	3nt-a*-3nt	5′–GUGAUCGCGCUUCUCGUUGGGG–3′

Table S1: scRNA sequences. (a) Forward mechanism (X ⊣ Y). (b) Reverse mechanism (Y ⊣ X). Sequences constrained by mRNA X (DsRed2) are shown in magenta; sequences constrained by mRNA Y (d2EGFP) are shown in green. Domain lengths: |a| = 16, |b| = 14, |c| = 5, |y| = 2, |z| = 19. Underlined nucleotides are 2′OMe-RNA; all other nucleotides are RNA. B oligonucleotides were constructed via ligation of B_1 and 5′-^{32}P labeled B_2 to incorporate ^{32}P into the backbone of B at the depicted location.

S3.2 mRNA sequences (X and Y)

The mRNA sequences were cloned into the pTnT vector for transcription with T7. The sequences were determined by isolating and sequencing mRNA from an HEK293 d2EGFP + DsRed2 cell line created in lab through genomic integration of pDsRed2-C1 (Clontech, PT3603-5, 632407) in HEK293 d2EGFP cells (gift from C. Beisel).

mRNA X: DsRed2
Nucleotides highlighted in magenta indicate the subsequence that the NUPACK sequence designer selected for detection by the scRNA for the forward mechanism (X ⊣ Y).

```
   1 GGUCAGAUCC GCUAGCGCUA CCGGUCGCCA CCAUGGCCUC CUCCGAGAAC GUCAUCACCG AGUUCAUGCG
  71 CUUCAAGGUG CGCAUGGAGG GCACCGUGAA CGGCCACGAG UUCGAGAUCG AGGGCGAGGG CGAGGGCCGC
 141 CCCUACGAGG GCCACAACAC CGUGAAGCUG AAGGUGACCA AGGGCGGCCC CCUGCCCUUC GCCUGGGACA
 211 UCCUGUCCCC CCAGUUCCAG UACGGCUCCA AGGUGUACGU GAAGCACCCC GCCGACAUCC CCGACUACAA
 281 GAAGCUGUCC UUCCCCGAGG GCUUCAAGUG GGAGCGCGUG AUGAACUUCG AGGACGGCGG CGUGGCGACC
 351 GUGACCCAGG ACUCCUCCCU GCAGGACGGC UGCUUCAUCU ACAAGGUGAA GUUCAUCGGC GUGAACUUCC
 421 CCUCCGACGG CCCCGUGAUG CAGAAGAAGA CCAUGGGCUG GGAGGCCUCC ACCGAGCGCC UGUACCCCCG
 491 CGACGGCGUG CUGAAGGGCG AGACCCACAA GGCCCUGAAG CUGAAGGACG GCGGCCACUA CCUGGUGGAG
 561 UUCAAGUCCA UCUACAUGGC CAAGAAGCCC GUGCAGCUGC CCGGCUACUA CUACGUGGAC GCCAAGCUGG
 631 ACAUCACCUC CCACAACGAG GACUACACCA UCGUGGAGCA GUACGAGCGC ACCGAGGGCC GCCACCACCU
 701 GUUCCUGAGA UCUCGAGCUC AAGCUUCGAA UUCUGCAGUC GACGGUACCG CGGGCCCGGG AUCCACCGGA
 771 UCUAGAUAAC UGAUCAUAAU CAGCCAUACC ACAUUUGUAG AGGUUUUACU UGCUUUAAAA AACCUCCCAC
 841 ACCUCCCCCU GAACCUGAAA CAUAAAAUGA AUGCAAUUGU UGUUGUUAAC UUGUUUAUUG CAGCUUAUAA
 911 UGGUUACAAA UAAAGCAAUA GCAUCACAAA UUUCACAAAU AAAGCAUUUU UUUCACUGCA AAAAAAAAAA
 981 AAAAAAAAAA AAAAAAAAAC UAG
```

mRNA Y: d2EGFP

Nucleotides highlighted in yellow indicate the accessible window identified using RNAhyb and supplied to the NUPACK sequence designer for design of the reverse mechanism (Y ⊣ X); nucleotides in green indicate the subsequence that the designer selected for detection by the scRNA.

```
   1 GAGAACCCAC UGCUUACUGG CUUAUCGAAA UUAAUACGAC UCACUAUAGG GAGACCCAAG CUGGCUAGCG
  71 UUUAAACUUA AGCUUGGUAC CCGCCACCAU GGUGAGCAAG GGCGAGGAGC UGUUCACCGG GGUGGUGCCC
 141 AUCCUGGUCG AGCUGGACGG CGACGUAAAC GGCCACAAGU UCAGCGUGUC CGGCGAGGGC GAGGGCGAUG
 211 CCACCUACGG CAAGCUGACC CUGAAGUUCA UCUGCACCAC CGGCAAGCUG CCCGUGCCCU GGCCCACCCU
 281 CGUGACCACC CUGACCUACG GCGUGCAGUG CUUCAGCCGC UACCCCGACC ACAUGAAGCA GCACGACUUC
 351 UUCAAGUCCG CCAUGCCCGA AGGCUACGUC CAGGAGCGCA CCAUCUUCUU CAAGGACGAC GGCAACUACA
 421 AGACCCGCGC CGAGGUGAAG UUCGAGGGCG ACACCCUGGU GAACCGCAUC GAGCUGAAGG GCAUCGACUU
 491 CAAGGAGGAC GGCAACAUCC UGGGGCACAA GCUGGAGUAC AACUACAACA GCCACAACGU CUAUAUCAUG
 561 GCCGACAAGC AGAAGAAUGG CAUCAAGGUG AACUUCAAGA UCCGCCACAA CAUCGAGGAC GGCAGCGUGC
 631 AGCUCGCCGA CCACUACCAG CAGAACACCC CCAUCGGCGA CGGCCCCGUG CUGCUGCCCG ACAACCACUA
 701 CCUGAGCACC CAGUCCGCCC UGAGCAAAGA CCCCAACGAG AAGCGCGAUC ACAUGGUCCU GCUGGAGUUC
 771 GUGACCGCCG CCGGGAUCAC UCUCGGCAUG GACGAGCUGU ACAAGAAGCU UAGCCAUGGC UUCCCGCCGG
 841 AGGUGGAGGA GCAGGAUGAU GGCACGCUGC CCAUGUCUUG UGCCCAGGAG AGCGGGAUGG ACCGUCACCC
 911 UGCAGCCUGU GCUUCUGCUA GGAUCAAUGU GUAGCUCGAG UCUAGAGGGC CCGUUUAAAC CCGCUGAUCA
 981 GCCUCGACUG UGCCUUCUAG UUGCCAGCCA UCUGUUGUUU GCCCCUCCCC CGUGCCUUCC UUGACCCUGG
1051 AAGGUGCCAC UCCCACUGUC CUUUCCUAAU AAAAUGAGGA AAUUGCAUCG CAAAAAAAAA AAAAAAAAAA
1121 AAAAAAAAAA ACUAG
```

S4 Motivating failures

S4.1 scRNA not functional with full-length mRNA input at low concentration in buffer or lysate (cf. Reference 1)

In Reference 1 (scRNA Mechanism 3), the scRNA that provided the starting point for the present work (see sequences in Table S2) was tested at 500 nM scRNA concentration in buffer (100 mM potassium acetate, 20 mM HEPES, pH 7.5; 37 °C for 2 h) with either a short RNA input X_s at 1× or a full-length mRNA input X at 2× (to account for uncertainties in mRNA concentration determination). Quantification of conditional production of shRNA B revealed an undetectable OFF state in the absence of an RNA input (i.e., smaller than the gel quantification uncertainty) and a strong ON state in the presence of either short RNA input X_s (> 200-fold increase) or full-length mRNA input X (> 50-fold increase).

Here, when the same scRNAs were tested at a lower 2.5 nM scRNA concentration in Buffer D– (20 mM HEPES, pH 7.5; 100 mM KCl; 0.2 mM EDTA, pH 8.0; 5% glycerol; 37 °C for 2 h) with RNA input at 4×, we observed strong conditional production of shRNA B in response to the short RNA input X_s but minimal production in response to full-length mRNA input X (Figure S4a). Furthermore, with the scRNA at 2.5 nM in 1.25 μg/μL of control lysate (37 °C for 2 h), there was diminished production of shRNA B in response to short RNA input X_s and negligible production in response to full-length mRNA input X (Figure S4b).

This loss of performance motivated domain redimensioning to recover scRNA performance using a full-length mRNA input at low concentration in lysate. Through multiple rounds of computational sequence design and experimental testing, we made the following modifications to the scRNA domain dimensions:

- increase toehold 'a' by 4 nt to improve nucleation with the full-length mRNA input,
- increase internal toeholds 'c' and 'c*' by 2 nt to improve self-nucleation within B during the hybridization cascade that leads to the formation of the shRNA Dicer substrate upon binding of scRNA A·B to mRNA input X
- addition of 2-nt duplex 'y/y*' to A·B to improve the OFF state (reduce spontaneous production of shRNA B in the absence of mRNA input X)

The redimensioned scRNA sequences for the forward mechanism (X ⊣ Y) are shown in Table S1a and are characterized in Figure 3a and 5.

scRNA tested in Figure S4

Strand	Domains	Sequence
X_s	a-b-c	5′–UGGGAGCGCGUGAUGAACUUCGAGGACGG–3′
A	z-c*-b*-a*	5′–UUCAUCUGCACCACCGGCACCGUCCUCGAAGUUCAUCACGCGCUCCCA–3′
B	z-c*-b-c-z*-y*	5′–UUCAUCUGCACCACCGGCACCGAUGAACUUCGAGGACGGUGCC^{32P}GGUGGUGCAGAUGAACU–3′
B_1		5′–UUCAUCUGCACCACCGGCACCGAUGAACUUCGAGGACGGUGCC–3′
B_2		5′–GGUGGUGCAGAUGAACU–3′

Table S2: Sequences for the previously studied scRNA of Reference 1. Sequences constrained by mRNA X (DsRed2) are shown in magenta; sequences constrained by mRNA Y (d2EGFP) are shown in green. Domain lengths: |a| = 12, |b| = 14, |c| = 3, |y| = 2, |z| = 19. Underlined nucleotides are 2′OMe-RNA; all other nucleotides are RNA. B oligonucleotides were constructed via ligation of B_1 and 5′-^{32}P labeled B_2 to incorporate ^{32}P into the backbone of B at the depicted location.

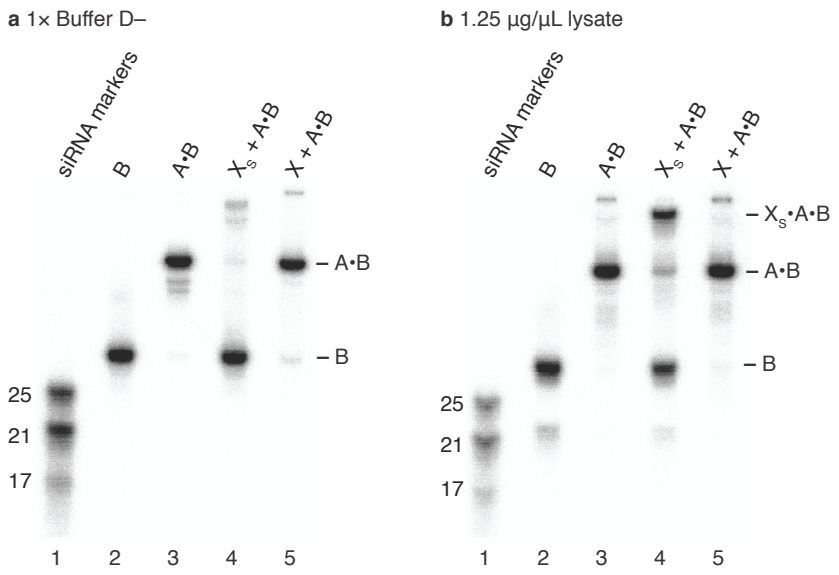

Figure S4: Testing previously studied scRNA at low concentration in buffer and lysate. The scRNA of Reference 1 (Mechanism 3) was tested at 2.5 nM in 1× Buffer D– (panel a) or 1.25 μg/μL control lysate (panel b). Experimental conditions: sequences of Table S2, strand B labeled with ^{32}P, reaction at 37°C for 2 h, 4× short RNA input X_s or full-length mRNA input X, separated via native PAGE after protein removal. With short RNA input X_s, production of shRNA B is nearly complete in buffer but reduced in lysate (lane 4). With full-length mRNA input X, production of shRNA B is minimal in buffer and negligible in lysate (lane 5). In lysate, the observed minimal processing of shRNA B into siRNAs could indicate that B is a poor Dicer substrate or that this batch of lysate has low Dicer activity.

S4.2 scRNAs functional in lysate for short RNA inputs but not full-length mRNA inputs

When designing the reverse mechanism (Y ⊣ X), we repeatedly encountered a situation where the designed scRNAs sequences functioned well in lysate, achieving strong conditional production of siRNA output anti-X when presented with short RNA input Y_s but not when presented with the full-length mRNA input Y. Sequences for two example designs with this property are shown in Table S3 and characterized in Figures S5 and S6. These difficulties resulting from the unpredictability of mRNA accessibility motivated the development of the RNAhyb assay (Section S2) to experimentally determine accessible windows within the full-length mRNA, which are then provided to the NUPACK designer as sequence constraints.

a scRNA tested in Figure S5

Strand	Domains	Sequence
Y_s	a-b-c	5′–AAGGACGACGGCAACUACAAGACCCGCGCCGAGGU–3′
A	y-z-c*-b*-a*	5′–UAGCAUCACAAAUUUCACAAAACCUCGGCGCGGGUCUUGUAGUUGCCGUCGUCCUU–3′
B	z-c*-b-c-z*-y*	5′–GCAUCACAAAUUUCACAAAACCUCACAAGACCCGCGCCGAGGUUUUGUGAA^{32P}AUUUGUGAUGCUA–3′
B_1		5′–GCAUCACAAAUUUCACAAAACCUCACAAGACCCGCGCCGAGGUUUUGUGAA–3′
B_2		5′–AUUUGUGAUGCUA–3′

b scRNA tested in Figure S6

Strand	Domains	Sequence
Y_s	a-b-c	5′–CAUGUCUUGUGCCCAGGAGAGCGGGAUGGACCGUC–3′
A	y-z-c*-b*-a*	5′–AUCACAAAUUUCACAAAUAAAGACGGUCCAUCCCGCUCUCCUGGGCACAAGACAUG–3′
B	z-c*-b-c-z*-y*	5′–CACAAAUUUCACAAAUAAAGACGGGAGAGCGGGAUGGACCGUCUUUAUUUG^{32P}UGAAAUUUGUGAU–3′
B_1		5′–CACAAAUUUCACAAAUAAAGACGGGAGAGCGGGAUGGACCGUCUUUAUUUG–3′
B_2		5′–UGAAAUUUGUGAU–3′

Table S3: Sequences for scRNAs that function in lysate for short RNA inputs but not full-length mRNA inputs. Sequences constrained by mRNA X (DsRed2) are shown in magenta; sequences constrained by mRNA Y (d2EGFP) are shown in green. Domain lengths: |a| = 16, |b| = 14, |c| = 5, |y| = 2, |z| = 19. Underlined nucleotides are 2′OMe-RNA; all other nucleotides are RNA. B oligonucleotides were constructed via ligation of B_1 and 5′-^{32}P labeled B_2 to incorporate ^{32}P into the backbone of B at the depicted location.

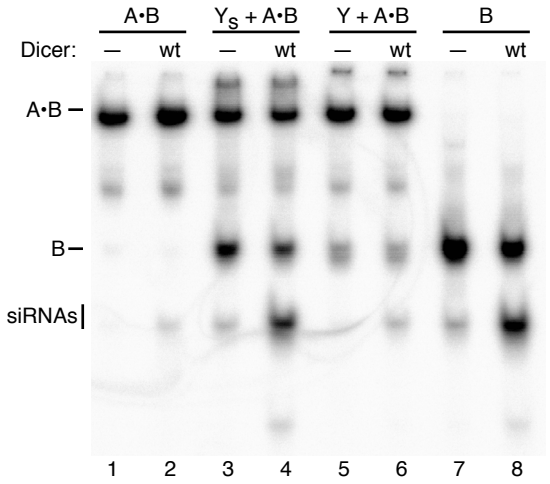

Figure S5: Example 1 of a preliminary reverse mechanism (Y ⊣ X) design where scRNA A·B responds to short RNA input Y_s but not full-length mRNA input Y. Experimental conditions: scRNA at 2.5 nM, sequences of Table S3a, strand B labeled with ^{32}P, 4× short RNA input Y_s or full-length mRNA input Y, reaction at 37 °C for 2 h in 1.25 μg/μL Dicer-depleted or wildtype lysate, separated via native PAGE after protein removal. Short RNA input Y_s triggers strong shRNA production in Dicer-depleted lysate (lane 3) and strong siRNA production in wildtype lysate (lane 4), but full-length mRNA input Y yields only weak shRNA and siRNA production (lanes 5 and 6); scRNA A·B predominantly does not bind to mRNA Y (lanes 5 and 6).

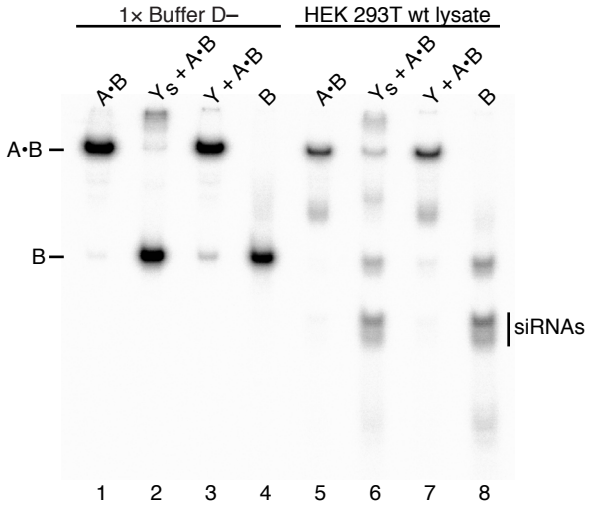

Figure S6: Example 2 of a preliminary reverse mechanism (Y ⊣ X) design where scRNA A·B responds to short RNA input Y_s but not full-length mRNA input Y. Experimental conditions: scRNA at 2.5 nM, sequences of Table S3b, strand B labeled with ^{32}P, 4× short RNA input Y_s or full-length mRNA input Y, reaction at 37 °C for 2 h in 1× Buffer D– (panel a) or 1.25 μg/μL wildtype lysate (panel b), separated via native PAGE after protein removal (reactions run in buffer were treated with the same conditions for consistency). scRNA A·B incubated with the short detection target Y_s produces shRNA B in buffer (lane 2) and siRNAs in lysate (lane 6), but A·B incubated with the full-length mRNA Y produces minimal shRNA B in buffer (lane 3) and negligible siRNA in lysate (lane 7).

S5 Additional scRNA signal transduction studies for forward and reverse mechanisms

Here, we present additional signal transduction controls for the forward mechanism (X ⊣ Y) and reverse mechanism (Y ⊣ X):

- Figure S7 displays stepping gels at high concentration (500 nM scRNA, 4× short RNA input) so that SYBR Gold staining can be used to image all strands.
- Figure S8 compares performance in Dicer-depleted lysate and in control lysate that undergoes the same preparation steps as the Dicer-depleted lysate (leaving out the Dicer siRNA and anti-Dicer antibody). scRNA performance in the control lysate is comparable to that in wildtype lysate (Figure 3), suggesting that the observed differences in Dicer processing between Dicer-depleted lysate and wildtype lysate are not an artifact of differences in lysate preparation steps.
- Figure S9 verifies that blocker strands do not interfere with scRNA performance, except via binding to the cognate mRNA input.
- Figure S10 provides replicates for quantification of conditional siRNA production.

S5.1 Stepping gels for forward and reverse mechanisms at high concentration in buffer with staining of all RNA species (cf. Figure 3)

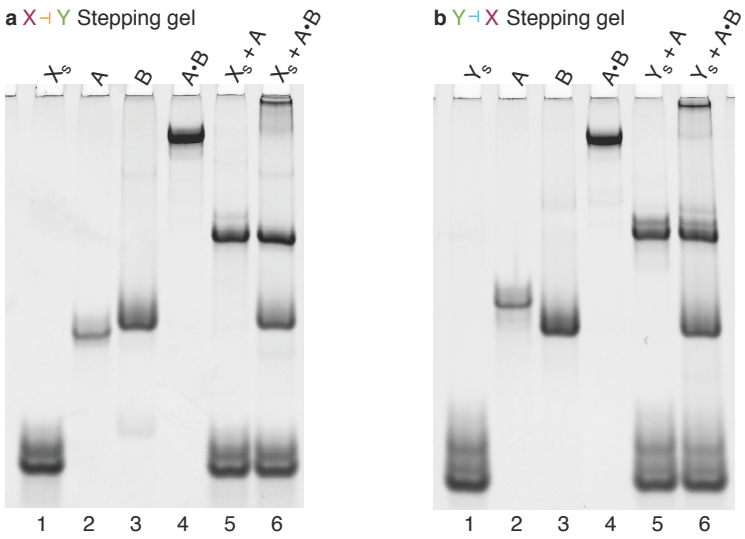

Figure S7: Stepping gels for forward and reverse mechanisms at high concentration in buffer with staining of all RNA species (cf. Figure 3). (a) Forward mechanism (X ⊣ Y). (b) Reverse mechanism (Y ⊣ X). Experimental conditions: scRNA at 500 nM, sequences of Table S1, 4× short RNA input X_s or Y_s, reaction at 37 °C for 4 h in 1× Buffer D–, separated via native PAGE, bands stained with SYBR Gold. A, B, X_s and Y_s serve as size markers (lanes 1–3). The scRNA duplex A·B forms a single band and no B is visible after the 4 h reaction (lane 4). Incubation of A with the cognate short RNA input (lane 5) yields duplex X_s·A (panel a) or Y_s·A (panel b). Incubation of scRNA A·B with the cognate short RNA input (lane 6) yields the shRNA B and duplex X_s·A (panel a) or Y_s·A (panel b) as well as a higher band that is likely the trimer X_s·A·B (panel a) or Y_s·A·B (panel b).

S5.2 Stepping gels for forward and reverse mechanisms in Dicer-depleted and control lysates (cf. Figure 3)

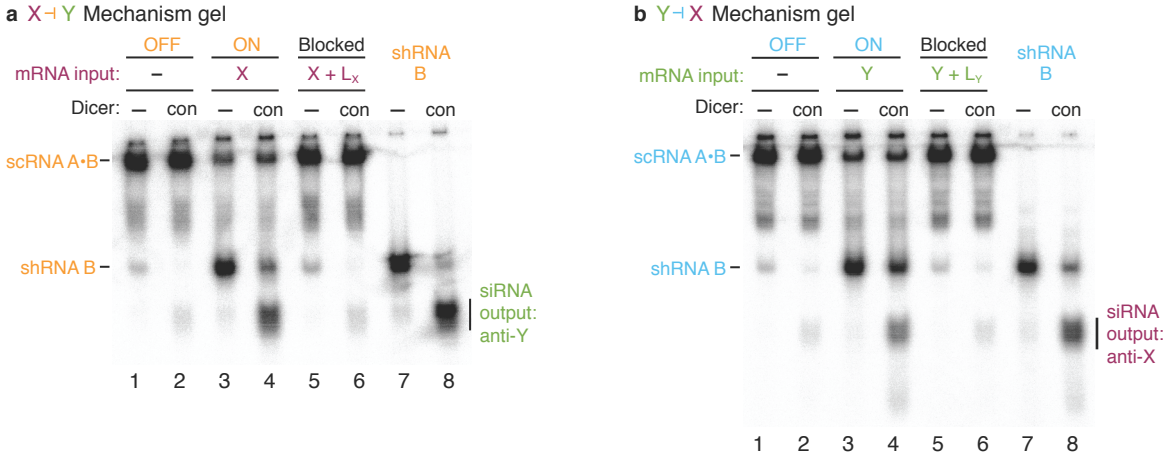

Figure S8: Stepping gels for forward and reverse mechanisms in Dicer-depleted and control lysates (cf. Figure 3). (a) Forward mechanism (X ⊣ Y). (b) Reverse mechanism (Y ⊣ X). Experimental conditions: scRNA at 2.5 nM, sequences of Table S1, strand B labeled with ^{32}P, 4× full-length mRNA input X (panel a) or Y (panel b), input mRNA pre-incubated with 2′OMe-RNA blocker strand for Blocked reactions, reaction at 37 °C for 4 h in 1.25 μg/μL Dicer-depleted lysate or control lysate (contains Dicer), separated via native PAGE. OFF state: in the absence of input mRNA, scRNA A·B is stable with minimal production of shRNA B Dicer substrate (lane 1) or siRNA following Dicer processing (lane 2). ON state: in the presence of the input mRNA, there is strong production of shRNA B (lane 3) and siRNA (lane 4). Blocked state: in the presence of a blocker strand that binds to the mRNA input at the scRNA nucleation site, the system is restored to the OFF sate (lanes 5, 6), indicating that the scRNA:mRNA interaction occurs at the intended location on the mRNA. shRNA B (lanes 7, 8) serves as a control for Dicer cleavage. The results in the control lysate are comparable to those obtained in wildtype lysate (Figure 3), with somewhat reduced Dicer efficiency for the reverse mechanism (lane 8 of panel b).

S5.3 Orthogonality gels for forward and reverse mechanisms with blocker strands (cf. Figures 3 and 5)

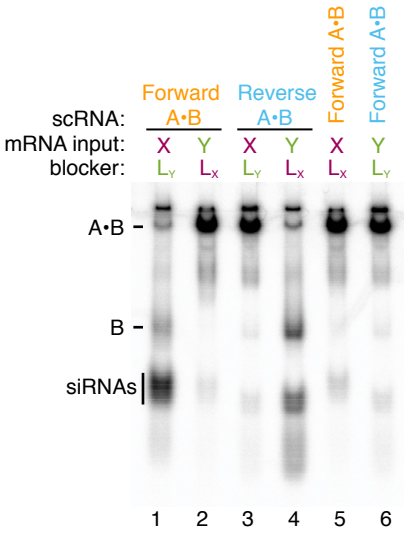

Figure S9: Orthogonality gels for forward and reverse mechanisms with blocker strands (cf. Figures 3 and 5). Blocker strands (L_X for mRNA input X for the forward mechanism, L_Y for mRNA input Y for the reverse mechanism) are complementary to the mRNA subsequence that serves as a nucleation site for the scRNA A·B. In lanes 1–4, the mRNA input is pre-incubated with the non-cognate blocker strand (X with L_Y, Y with L_X); in lanes 5-6, the mRNA input is pre-incubated with the cognate clocker strand (X with L_X, Y with L_Y). Experimental conditions: scRNAs at 2.5 nM, sequences of Table S1, B strands labeled with ^{32}P, 4× full-length mRNA input X or Y, input mRNA pre-incubated with indicated 2′OMe-RNA blocker strand, reaction at 37 °C for 4 h in 1.25 μg/μL wildtype lysate (containing endogenous Dicer), separated via native PAGE. As expected, the non-cognate blocker strands do not significantly alter the ability of the cognate mRNA input to trigger siRNA production (forward mechanism, lane 1; reverse mechanism, lane 4). Furthermore, the non-cognate blocker strands do not significantly alter the inability of the non-cognate mRNA input to trigger siRNA production (forward mechanism, lane 2; reverse mechanism, lane 3).

S5.4 Orthogonality gel replicates for forward and reverse mechanisms in lysate (cf. Figure 5)

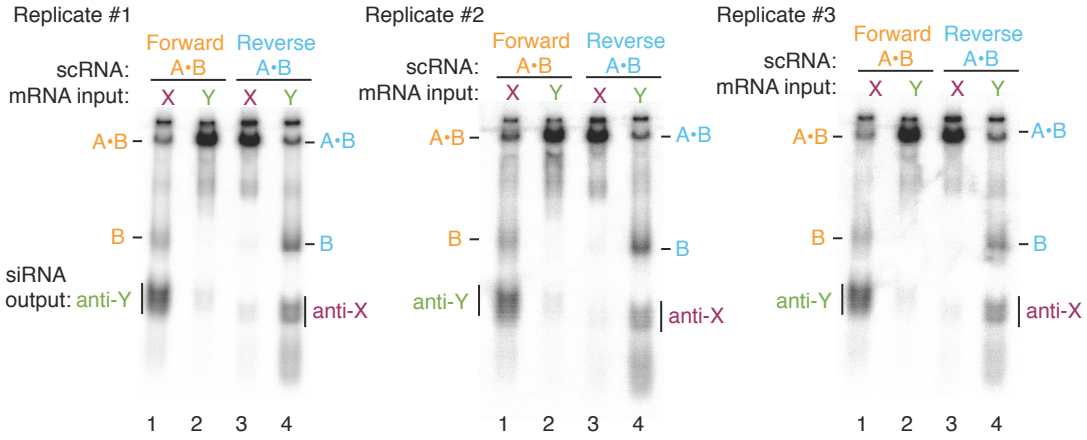

Figure S10: Orthogonality gel replicates for forward and reverse mechanisms in lysate (cf. Figure 5). Conditional siRNA production in the presence of cognate mRNA input (ON state) or non-cognate mRNA input (OFF state) for forward logic (X ⊣ Y: cognate mRNA input X, siRNA output anti-Y, non-cognate mRNA input Y) and reverse logic (Y ⊣ X: cognate mRNA input Y, siRNA output anti-X, non-cognate mRNA input X). Experimental conditions: scRNAs at 2.5 nM, sequences of Table S1, B strands labeled with ^{32}P, 4× full-length mRNA input X or Y, reaction at 37 °C for 4 h in 1.25 μg/μL wildtype lysate (containing endogenous Dicer), separated via native PAGE. OFF state: minimal siRNA production in the presence of non-cognate mRNA input (lanes 2 and 3). ON state: strong production in the presence of cognate mRNA input (lanes 1 and 4).

S6 RNAhyb studies

Here, we present RNAhyb studies (protocol of Section S2) that were used to identify accessible subsequences of mRNA input Y to provide to the NUPACK designer as sequence constraints when designing the scRNA sequences for the reverse mechanism ($Y \dashv X$):

- Table S4 presents 20-nt mRNA subsequences, the complementary 20-nt DNA probe sequences, and the probe hybridization yield for 1–3 replicate gels. Figure S11 provides an expanded view of the data from Figure 4 in the main text, depicting the probe hybridization yield for each probe, as well as the mRNA window provided to the NUPACK designer following inspection of the RNAhyb data, and the scRNA binding site selected by NUPACK within this window. Probe hybridization yields ranged from 0 to $\approx$40%, indicating the challenge of detecting short subsequences in the context of a full-length mRNA. Accessibility in vivo may differ due to the presence of RNA-binding proteins and helicase activity.[10]
- Figures S12 and S13 demonstrate the appearance of typical RNAhyb gels.
- Figure S14 compares probe hybridization yield experimental data to three types of mRNA accessibility predictions calculated using NUPACK. To reduce overall experimental effort, these data suggest the approach of first computationally screening the mRNA subsequences to identify those with low subsequence free energy (corresponding to minimal predicted secondary structure), and then using the RNAhyb assay to experimentally identify accessible windows from within this reduced set of subsequences.

The RNAhyb assay employs DNA probes rather than RNA or 2′OMe-RNA probes due to the much lower cost of DNA synthesis. However, DNA:RNA base-pairing[11] is weaker than RNA:RNA base-pairing[12] and 2′OMe-RNA:RNA base-pairing,[13] so mRNA:probe binding should provide a conservative estimate of mRNA accessibility.

S6.1 mRNA subsequences, probe sequences, and probe hybridization yields

Start position	mRNA window sequence	DNA probe sequence	Fraction probe bound		
			Rep 1	Rep 2	Rep 3
1	GAGAACCCACUGCUUACUGG	CCAGTAAGCAGTGGGTTCTC	0.06		
11	UGCUUACUGGCUUAUCGAAA	TTTCGATAAGCCAGTAAGCA	0.02		
21	CUUAUCGAAAUUAAUACGAC	GTCGTATTAATTTCGATAAG	0.01		
31	UUAAUACGACUCACUAUAGG	CCTATAGTGAGTCGTATTAA	0.01		
41	UCACUAUAGGGAGACCCAAG	CTTGGGTCTCCCTATAGTGA	0.02		
51	GAGACCCAAGCUGGCUAGCG	CGCTAGCCAGCTTGGGTCTC	0.05		
61	CUGGCUAGCGUUUAAACUUA	TAAGTTTAAACGCTAGCCAG	0.02		
71	UUUAAACUUAAGCUUGGUAC	GTACCAAGCTTAAGTTTAAA	0.00		
81	AGCUUGGUACCCGCCACCAU	ATGGTGGCGGGTACCAAGCT	0.07		
91	CCGCCACCAUGGUGAGCAAG	CTTGCTCACCATGGTGGCGG	0.01		
101	GGUGAGCAAGGGCGAGGAGC	GCTCCTCGCCCTTGCTCACC	0.07		
111	GGCGAGGAGCUGUUCACCGG	CCGGTGAACAGCTCCTCGCC	0.01		
121	UGUUCACCGGGGUGGUGCCC	GGGCACCACCCCGGTGAACA	0.00		
131	GGUGGUGCCCAUCCUGGUCG	CGACCAGGATGGGCACCACC	0.00		
141	AUCCUGGUCGAGCUGGACGG	CCGTCCAGCTCGACCAGGAT	0.00		
151	AGCUGGACGGCGACGUAAAC	GTTTACGTCGCCGTCCAGCT	0.00		
161	CGACGUAAACGGCCACAAGU	ACTTGTGGCCGTTTACGTCG	0.00		
171	GGCCACAAGUUCAGCGUGUC	GACACGCTGAACTTGTGGCC	0.00		
181	UCAGCGUGUCCGGCGAGGGC	GCCCTCGCCGGACACGCTGA	0.00		
191	CGGCGAGGGCGAGGGCGAUG	CATCGCCCTCGCCCTCGCCG	0.00		
201	GAGGGCGAUGCCACCUACGG	CCGTAGGTGGCATCGCCCTC	0.00		
211	CCACCUACGGCAAGCUGACC	GGTCAGCTTGCCGTAGGTGG	0.03		
221	CAAGCUGACCCUGAAGUUCA	TGAACTTCAGGGTCAGCTTG	0.01		
231	CUGAAGUUCAUCUGCACCAC	GTGGTGCAGATGAACTTCAG	0.02		
241	UCUGCACCACCGGCAAGCUG	CAGCTTGCCGGTGGTGCAGA	0.02		
251	CGGCAAGCUGCCCGUGCCCU	AGGGCACGGGCAGCTTGCCG	0.01		
261	CCCGUGCCCUGGCCCACCCU	AGGGTGGGCCAGGGCACGGG	0.00		
271	GGCCCACCCUCGUGACCACC	GGTGGTCACGAGGGTGGGCC	0.01		
281	CGUGACCACCCUGACCUACG	CGTAGGTCAGGGTGGTCACG	0.02		
291	CUGACCUACGGCGUGCAGUG	CACTGCACGCCGTAGGTCAG	0.00		
301	GCGUGCAGUGCUUCAGCCGC	GCGGCTGAAGCACTGCACGC	0.00		
311	CUUCAGCCGCUACCCCGACC	GGTCGGGGTAGCGGCTGAAG	0.14	0.16	
321	UACCCCGACCACAUGAAGCA	TGCTTCATGTGGTCGGGGTA	0.11	0.11	
331	ACAUGAAGCAGCACGACUUC	GAAGTCGTGCTGCTTCATGT	0.00		
341	GCACGACUUCUUCAAGUCCG	CGGACTTGAAGAAGTCGTGC	0.01		
351	UUCAAGUCCGCCAUGCCCGA	TCGGGCATGGCGGACTTGAA	0.01		
361	CCAUGCCCGAAGGCUACGUC	GACGTAGCCTTCGGGCATGG	0.01		
371	AGGCUACGUCCAGGAGCGCA	TGCGCTCCTGGACGTAGCCT	0.01		
381	CAGGAGCGCACCAUCUUCUU	AAGAAGATGGTGCGCTCCTG	0.04		
391	CCAUCUUCUUCAAGGACGAC	GTCGTCCTTGAAGAAGATGG	0.02		
401	CAAGGACGACGGCAACUACA	TGTAGTTGCCGTCGTCCTTG	0.08		
411	GGCAACUACAAGACCCGCGC	GCGCGGGTCTTGTAGTTGCC	0.11	0.11	
421	AGACCCGCGCCGAGGUGAAG	CTTCACCTCGGCGCGGGTCT	0.02		
431	CGAGGUGAAGUUCGAGGGCG	CGCCCTCGAACTTCACCTCG	0.01		
441	UUCGAGGGCGACACCCUGGU	ACCAGGGTGTCGCCCTCGAA	0.00		
451	ACACCCUGGUGAACCGCAUC	GATGCGGTTCACCAGGGTGT	0.02		
461	GAACCGCAUCGAGCUGAAGG	CCTTCAGCTCGATGCGGTTC	0.00		
471	GAGCUGAAGGGCAUCGACUU	AAGTCGATGCCCTTCAGCTC	0.03		
481	GCAUCGACUUCAAGGAGGAC	GTCCTCCTTGAAGTCGATGC	0.02		
491	CAAGGAGGACGGCAACAUCC	GGATGTTGCCGTCCTCCTTG	0.03		
501	GGCAACAUCCUGGGGCACAA	TTGTGCCCCAGGATGTTGCC	0.00		
511	UGGGGCACAAGCUGGAGUAC	GTACTCCAGCTTGTGCCCCA	0.02		
521	GCUGGAGUACAACUACAACA	TGTTGTAGTTGTACTCCAGC	0.06		
531	AACUACAACAGCCACAACGU	ACGTTGTGGCTGTTGTAGTT	0.06		
541	GCCACAACGUCUAUAUCAUG	CATGATATAGACGTTGTGGC	0.04		
551	CUAUAUCAUGGCCGACAAGC	GCTTGTCGGCCATGATATAG	0.03		
561	GCCGACAAGCAGAAGAAUGG	CCATTCTTCTGCTTGTCGGC	0.05		
571	AGAAGAAUGGCAUCAAGGUG	CACCTTGATGCCATTCTTCT	0.02		
581	CAUCAAGGUGAACUUCAAGA	TCTTGAAGTTCACCTTGATG	0.04		
591	AACUUCAAGAUCCGCCACAA	TTGTGGCGGATCTTGAAGTT	0.08		
601	UCCGCCACAACAUCGAGGAC	GTCCTCGATGTTGTGGCGGA	0.08		
611	CAUCGAGGACGGCAGCGUGC	GCACGCTGCCGTCCTCGATG	0.02		
621	GGCAGCGUGCAGCUCGCCGA	TCGGCGAGCTGCACGCTGCC	0.00		
631	AGCUCGCCGACCACUACCAG	CTGGTAGTGGTCGGCGAGCT	0.09		
641	CCACUACCAGCAGAACACCC	GGGTGTTCTGCTGGTAGTGG	0.38	0.28	
651	CAGAACACCCCCAUCGGCGA	TCGCCGATGGGGGTGTTCTG	0.16	0.22	

Start position	mRNA window sequence	DNA probe sequence	Fraction probe bound Rep 1	Rep 2	Rep 3
661	CCAUCGGCGACGGCCCCGUG	CACGGGGCCGTCGCCGATGG	0.02		
666	GGCGACGGCCCCGUGCUGCU	AGCAGCACGGGGCCGTCGCC	0.04		
671	CGGCCCCGUGCUGCUGCCCG	CGGGCAGCAGCACGGGGCCG	0.01	0.04	
676	CCGUGCUGCUGCCCGACAAC	GTTGTCGGGCAGCAGCACGG	0.13		
681	CUGCUGCCCGACAACCACUA	TAGTGGTTGTCGGGCAGCAG	0.14	0.13	
686	GCCCGACAACCACUACCUGA	TCAGGTAGTGGTTGTCGGGC	0.15		
691	ACAACCACUACCUGAGCACC	GGTGCTCAGGTAGTGGTTGT	0.13	0.17	0.25
696	CACUACCUGAGCACCCAGUC	GACTGGGTGCTCAGGTAGTG	0.21		
701	CCUGAGCACCCAGUCCGCCC	GGGCGGACTGGGTGCTCAGG	0.27	0.26	
706	GCACCCAGUCCGCCCUGAGC	GCTCAGGGCGGACTGGGTGC	0.25		
711	CAGUCCGCCCUGAGCAAAGA	TCTTTGCTCAGGGCGGACTG	0.09	0.13	
716	CGCCCUGAGCAAAGACCCCA	TGGGGTCTTTGCTCAGGGCG	0.25		
721	UGAGCAAAGACCCCAACGAG	CTCGTTGGGGTCTTTGCTCA	0.13	0.10	
726	AAAGACCCCAACGAGAAGCG	CGCTTCTCGTTGGGGTCTTT	0.15		
731	CCCCAACGAGAAGCGCGAUC	GATCGCGCTTCTCGTTGGGG	0.09	0.14	
734	CAACGAGAAGCGCGAUCACA	TGTGATCGCGCTTCTCGTTG	0.10		
736	ACGAGAAGCGCGAUCACAUG	CATGTGATCGCGCTTCTCGT	0.06		
741	AAGCGCGAUCACAUGGUCCU	AGGACCATGTGATCGCGCTT	0.04		
751	ACAUGGUCCUGCUGGAGUUC	GAACTCCAGCAGGACCATGT	0.00		
761	GCUGGAGUUCGUGACCGCCG	CGGCGGTCACGAACTCCAGC	0.01		
771	GUGACCGCCGCCGGGAUCAC	GTGATCCCGGCGGCGGTCAC	0.00		
781	CCGGGAUCACUCUCGGCAUG	CATGCCGAGAGTGATCCCGG	0.00		
791	UCUCGGCAUGGACGAGCUGU	ACAGCTCGTCCATGCCGAGA	0.00		
801	GACGAGCUGUACAAGAAGCU	AGCTTCTTGTACAGCTCGTC	0.01		
811	ACAAGAAGCUUAGCCAUGGC	GCCATGGCTAAGCTTCTTGT	0.01		
821	UAGCCAUGGCUUCCCGCCGG	CCGGCGGGAAGCCATGGCTA	0.04		
831	UUCCCGCCGGAGGUGGAGGA	TCCTCCACCTCCGGCGGGAA	0.00		
841	AGGUGGAGGAGCAGGAUGAU	ATCATCCTGCTCCTCCACCT	0.03		
851	GCAGGAUGAUGGCACGCUGC	GCAGCGTGCCATCATCCTGC	0.00		
861	GGCACGCUGCCCAUGUCUUG	CAAGACATGGGCAGCGTGCC	0.00		
871	CCAUGUCUUGUGCCCAGGAG	CTCCTGGGCACAAGACATGG	0.01		
881	UGCCCAGGAGAGCGGGAUGG	CCATCCCGCTCTCCTGGGCA	0.04		
891	AGCGGGAUGGACCGUCACCC	GGGTGACGGTCCATCCCGCT	0.01		
901	ACCGUCACCCUGCAGCCUGU	ACAGGCTGCAGGGTGACGGT	0.01		
911	UGCAGCCUGUGCUUCUGCUA	TAGCAGAAGCACAGGCTGCA	0.00		
921	GCUUCUGCUAGGAUCAAUGU	ACATTGATCCTAGCAGAAGC	0.03		
931	GGAUCAAUGUGUAGCUCGAG	CTCGAGCTACACATTGATCC	0.01		
941	GUAGCUCGAGUCUAGAGGGC	GCCCTCTAGACTCGAGCTAC	0.05		
951	UCUAGAGGGCCCGUUUAAAC	GTTTAAACGGGCCCTCTAGA	0.04		
961	CCGUUUAAACCCGCUGAUCA	TGATCAGCGGGTTTAAACGG	0.05		
971	CCGCUGAUCAGCCUCGACUG	CAGTCGAGGCTGATCAGCGG	0.03		
981	GCCUCGACUGUGCCUUCUAG	CTAGAAGGCACAGTCGAGGC	0.01		
991	UGCCUUCUAGUUGCCAGCCA	TGGCTGGCAACTAGAAGGCA	0.01		
1001	UUGCCAGCCAUCUGUUGUUU	AAACAACAGATGGCTGGCAA	0.04		
1011	UCUGUUGUUUGCCCCUCCCC	GGGGAGGGGCAAACAACAGA	0.15	0.22	
1021	GCCCCUCCCCCGUGCCUUCC	GGAAGGCACGGGGGAGGGGC	0.08		
1031	CGUGCCUUCCUUGACCCUGG	CCAGGGTCAAGGAAGGCACG	0.04		
1041	UUGACCCUGGAAGGUGCCAC	GTGGCACCTTCCAGGGTCAA	0.04		
1051	AAGGUGCCACUCCCACUGUC	GACAGTGGGAGTGGCACCTT	0.11	0.25	
1061	UCCCACUGUCCUUUCCUAAU	ATTAGGAAAGGACAGTGGGA	0.13	0.11	
1071	CUUUCCUAAUAAAAUGAGGA	TCCTCATTTTATTAGGAAAG	0.01		
1081	AAAAUGAGGAAAUUGCAUCG	CGATGCAATTTCCTCATTTT	0.08	0.05	

Table S4: RNAhyb sequences and mRNA:probe hybridization yields for mRNA Y (d2EGFP). Columns: window start position within mRNA, mRNA window sequence, DNA probe sequence (complementary to mRNA window), and fraction of probe bound for up to 3 replicate experiments. The ^{32}P-labeled DNA probe is the limiting species (DNA probe = 2.5 nM, mRNA = 10 nM). Generally, the probes with the best binding were included in replicate experiments. For some probes with higher yield, there is significant variation between replicates, suggesting high sensitivity to experimental conditions. Sequences listed 5′ to 3′.

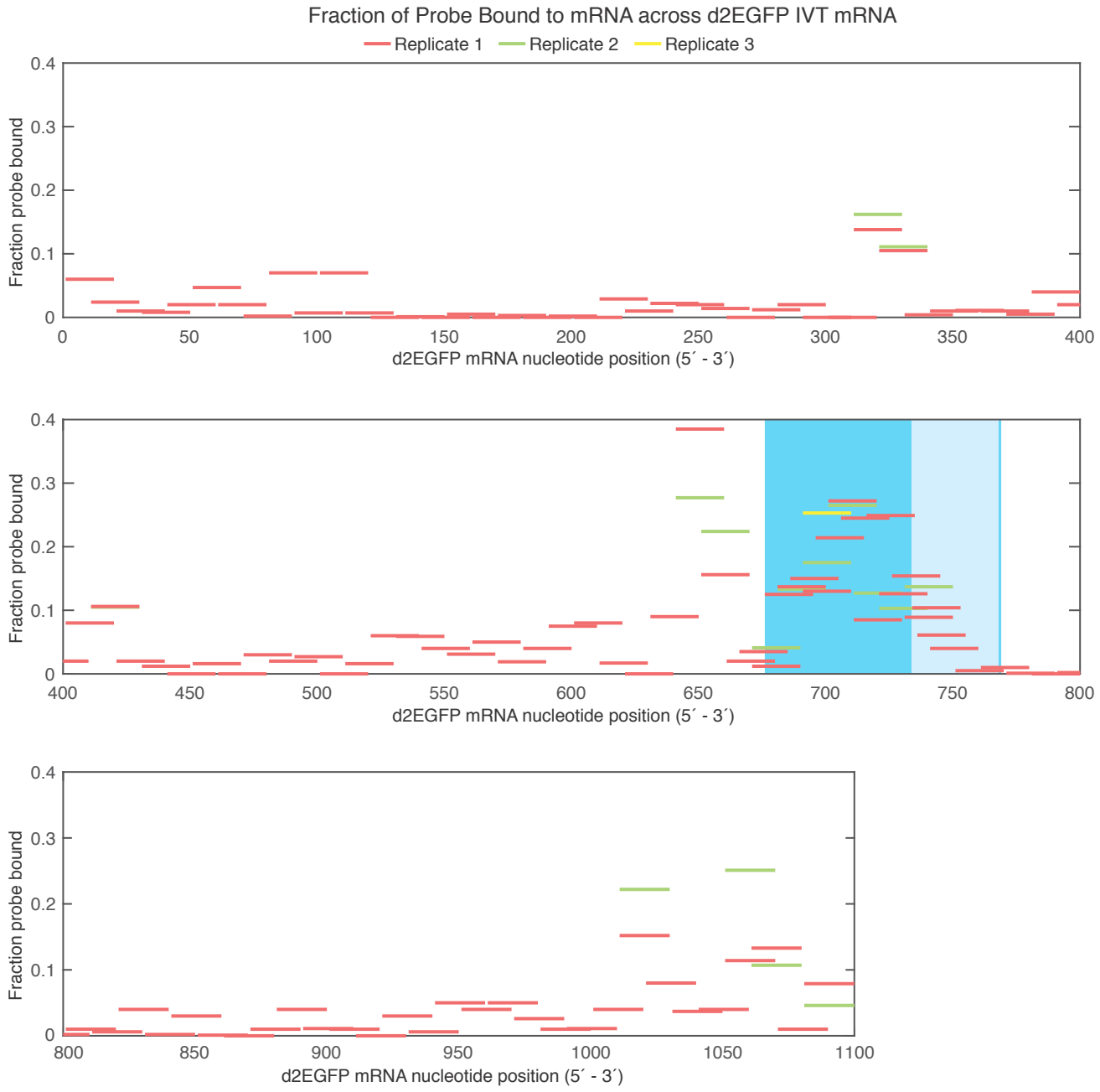

Figure S11: RNAhyb fraction of probe bound for mRNA Y (d2EGFP). Each plotted line depicts the location of a probe along the mRNA (abscissa) and the fraction of probe bound to the mRNA (ordinate). The ^{32}P-labeled DNA probe is the limiting species (DNA probe = 2.5 nM, mRNA = 10 nM). All probes were tested at least once, with some probes tested up to three times. The region between 676 and 769 (medium blue shading) was provided to the NUPACK designer as an accessible window when designing the reverse mechanism (Y $\dashv$ X). The light blue shading indicates the mRNA window selected by NUPACK for scRNA binding.

S6.2 Example gels demonstrating range of probe hybridization yields

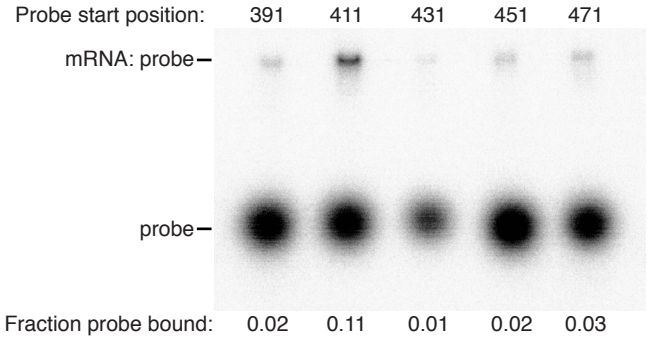

Figure S12: Example RNAhyb gel 1. For each probe, the mRNA and 20-nt ^{32}P-labeled DNA probe were incubated together for 2 h at 37 °C (DNA probe = 2.5 nM, mRNA = 10 nM) and then analyzed by native PAGE. The fraction of probe bound was calculated by dividing the background-subtracted signal of the mRNA:probe band by the background-subtracted total signal for the lane. In this example, only one of the probes has binding greater than 10% (probe 411). The total lane signal for probe 431 is visibly lower than for the other probes due to differences in T4 PNK 5′-phosphorylation efficiency, which is influenced by both sequence and structure.[14]

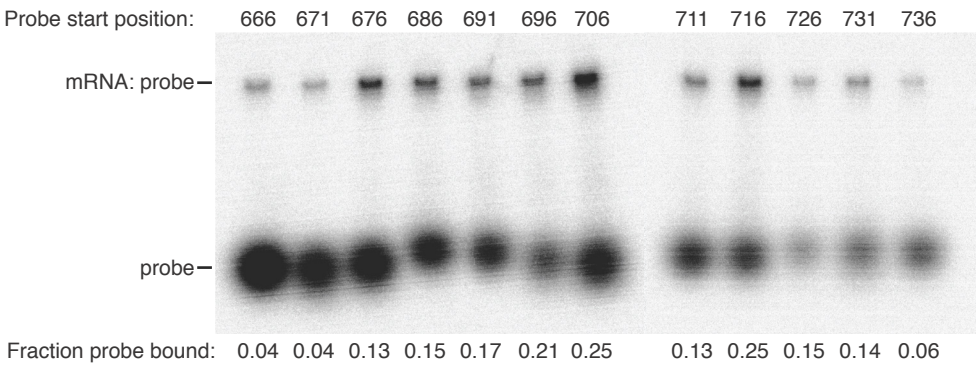

Figure S13: Example RNAhyb gel 2: a representative gel quantifying mRNA accessibility. Here, we tested additional probes in a relatively accessible region of the mRNA. For each probe, the mRNA and 20-nt ^{32}P-labeled DNA probe were incubated together for 2 h at 37 °C (DNA probe = 2.5 nM, mRNA = 10 nM) and then analyzed by native PAGE. The fraction of probe bound was calculated by dividing the background-subtracted signal of the mRNA:probe band by the background-subtracted total signal for the lane.

S6.3 Comparison of experimental hybridization yields (RNAhyb) and computational accessibility predictions (NUPACK) for mRNA input Y (d2EGFP)

Figure S14 compares RNAhyb probe hybridization yield against three computational proxies for mRNA accessibility calculated using NUPACK: mRNA subsequence free energy, mRNA subsequence average equilibrium probability unpaired, equilibrium fraction probe bound.

Using mRNA subsequence free energy (Figure S14a), it is striking that the data fall reliably in the lower right triangle. Subsequences predicted to be inaccessible computationally (say $\Delta G < -3$ kcal/mol) are indeed shown to be poor binders experimentally. On the other hand, subsequences predicted to be accessible computationally (say $-3 \leq \Delta G \leq 0$ kcal/mol) need to be tested experimentally in order to find the subset that are indeed good binders. To reduce overall experimental effort, these data suggest the approach of first computationally screening the mRNA subsequences to identify those with $-3 \leq \Delta G \leq 0$ kcal/mol and then using the RNAhyb gel assay to experimentally identify accessible windows from within this reduced set of subsequences; further study is warranted. In the context of the full-length mRNA, there will be base-pairing between subsequences as well as within subsequences, so the present approach of examining the free energy of each subsequence represents only a simple computational proxy for accessibility.

The other computational proxies do not provide useful information. Average equilibrium fraction unpaired (Figure S14b) produces both high and low values for the good binders, and hence does not provide a basis for narrowing the field in the search for good binders. Equilibrium fraction probe bound (Figure S14c) is predicted to be high for all probes, hence is not useful in discriminating between good and bad binders; note that the RNAhyb experiments use DNA probes (to reduce cost) and the NUPACK calculations use RNA probes (because NUPACK does not include parameters for DNA:RNA interactions), which reduces the comparability of the experimental and computational hybridization yields. The NUPACK calculations also do not take into account pseudoknots, tertiary structure effects, and kinetic effects, all of which may contribute to the measured experimental binding properties.

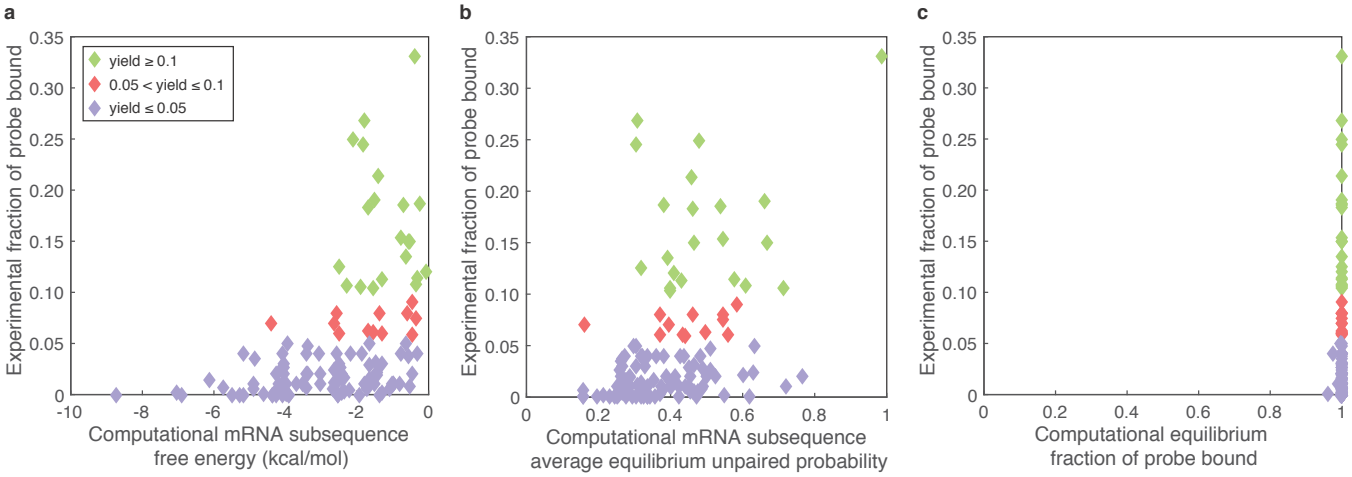

Figure S14: Comparison of experimental hybridization yields (RNAhyb) and computational accessibility predictions (NUPACK) for mRNA input Y (d2EGFP). (a) Experimental fraction probe bound (mean over replicates of Table S4 and Figure S11) vs computed mRNA subsequence free energy ($\Delta G \equiv -k_B T \log Q$, where Q is the partition function over the ensemble of all unpseudoknotted secondary structures for the 20-nt mRNA subsequence, k_B is the Boltzmann constant, and T is temperature). $\Delta G \approx 0$ for a window predicted to have negligible base-pairing, ΔG becomes increasingly negative as the probability of equilibrium base-pairing increases. Calculations performed for one 20-nt mRNA subsequence at a time in 1M Na^+ at 37 °C.[4] (b) Experimental fraction probe bound vs computed mRNA subsequence average equilibrium unpaired probability (the equilibrium probability of being unpaired averaged over each 20-nt subsequence). Calculation performed for full mRNA in 1M Na^+ at 37 °C[4] followed by averaging over 20 nt for each subsequence. (c) Experimental fraction probe bound vs computed equilibrium fraction probe bound. Note that the experiments use DNA probes (to reduce cost) and the calculations use RNA probes (because NUPACK does not include parameters for DNA:RNA interactions). Calculations performed for one RNA probe at a time (2.5 nM) together with full mRNA (10 nM) in 1M Na^+ at 37 °C.[4]

S7 Chemical modification studies

Initially, we performed all scRNA studies using 2′OMe-RNA for strand A (to prevent Dicer processing of scRNA A·B) and unmodified RNA for strand B (to permit Dicer processing of shRNA B). However, for the reverse mechanism (Y ⊣ X), strand B was rapidly degraded when scRNA A·B was introduced into lysate (Figure S15, modification M0); interestingly, the same strand was considerably more resistant to degradation when in shRNA form. Modifying B is challenging because the modifications must protect B from degradation in the lysate (including in the A·B scRNA complex), but still allow Dicer to cleave shRNA B into siRNAs. Thus, the strategy of using 2′OMe-RNA for B, which was our solution for protecting A from degradation, was not feasible since it interferes with Dicer cleavage (Figure S15, modification M1). We tested a number of modifications for the reverse mechanism (Figure S15 and Table S6) before discovering that using 1 nt of 2′OMe-RNA at each end of B was sufficient to provide good protection against degradation while permitting efficient Dicer processing. The same 1-nt end modifications also proved to work well for the forward mechanism (Figure S16).

S7.1 Sequence composition of tested chemical modifications

a Forward mechanism (X ⊣ Y)

Modification	Strand	Sequence
M0	B	5′–UUCAAGAUCCGCCACAACAGAUGCCAAAUAAAGCAAUAGCAUCUGUUGUGGC^{32P}GGAUCUUGAAGU–3′
M0	B_1	5′–UUCAAGAUCCGCCACAACAGAUGCCAAAUAAAGCAAUAGCAUCUGUUGUGGC–3′
M0	B_2	5′–GGAUCUUGAAGU–3′
M6	B	5′–UUCAAGAUCCGCCACAACAGAUGCCAAAUAAAGCAAUAGCAUCUGUUGUGGC^{32P}GGAUCUUGAAGU–3′
M6	B_1	5′–UUCAAGAUCCGCCACAACAGAUGCCAAAUAAAGCAAUAGCAUCUGUUGUGGC–3′
M6	B_2	5′–GGAUCUUGAAGU–3′

b Reverse mechanism (Y ⊣ X)

Modification	Strand	Sequence
M0	B	5′–CAUCACAAAUUUCACAAAUACUCCCACAUGGUCCUGCUGGAGUAUUUGU^{32P}GAAAUUUGUGAUGCU–3′
M0	B_1	5′–CAUCACAAAUUUCACAAAUACUCCCACAUGGUCCUGCUGGAGUAUUUGU–3′
M0	B_2	5′–GAAAUUUGUGAUGCU–3′
M1	B	5′–CAUCACAAAUUUCACAAAUACUCCCACAUGGUCCUGCUGGAGUAUUUGU^{32P}GAAAUUUGUGAUGCU–3′
M1	B_1	5′–CAUCACAAAUUUCACAAAUACUCCCACAUGGUCCUGCUGGAGUAUUUGU–3′
M1	B_2	5′–GAAAUUUGUGAUGCU–3′
M2	B	5′–CAUCACAAAUUUCACAAAUACUCCCACAUGGUCCUGCUGGAGUAUUUGU^{32P}GAAAUUUGUGAUGCU–3′
M2	B_1	5′–CAUCACAAAUUUCACAAAUACUCCCACAUGGUCCUGCUGGAGUAUUUGU–3′
M2	B_2	5′–GAAAUUUGUGAUGCU–3′
M3	B	5′–C$^{\#}$A$^{\#}$U$^{\#}$CACAAAUUUCACAAAUACUCCCACAUGGUCCUGCUGGAGUAUUUGU^{32P}GAAAUUUGUGAU$^{\#}$G$^{\#}$C$^{\#}$U–3′
M3	B_1	5′–C$^{\#}$A$^{\#}$U$^{\#}$CACAAAUUUCACAAAUACUCCCACAUGGUCCUGCUGGAGUAUUUGU–3′
M3	B_2	5′–GAAAUUUGUGAU$^{\#}$G$^{\#}$C$^{\#}$U–3′
M4	B	5′–CAUCACAAAUUUCACAAAUACUCCCACAUGGUCCUGCUGGAGUAUUUGU^{32P}GAAAUUUGUGAUGCU–3′
M4	B_1	5′–CAUCACAAAUUUCACAAAUACUCCCACAUGGUCCUGCUGGAGUAUUUGU–3′
M4	B_2	5′–GAAAUUUGUGAUGCU–3′ (same as M0 B_2)
M5	B	5′–CAUCACAAAUUUCACAAAUACUCCCACAUGGUCCUGCUGGAGUAUUUGU^{32P}GAAAUUUGUGAUGdTdT–3′
M5	B_1	5′–CAUCACAAAUUUCACAAAUACUCCCACAUGGUCCUGCUGGAGUAUUUGU–3′ (same as M0 B_1)
M5	B_2	5′–GAAAUUUGUGAUGdTdT–3′
M6	B	5′–CAUCACAAAUUUCACAAAUACUCCCACAUGGUCCUGCUGGAGUAUUUGU^{32P}GAAAUUUGUGAUGCU–3′
M6	B_1	5′–CAUCACAAAUUUCACAAAUACUCCCACAUGGUCCUGCUGGAGUAUUUGU–3′
M6	B_2	5′–GAAAUUUGUGAUGCU–3′

Table S5: Chemical modifications tested for shRNA B. (a) Forward mechanism (X ⊣ Y). (b) Reverse mechanism (Y ⊣ X). Sequences constrained by mRNA X (DsRed2) are shown in magenta; sequences constrained by mRNA Y (d2EGFP) are shown in green. 2′OMe-RNA nucleotides are underlined. DNA nucleotides are indicated by the prefix 'd'. Phosphorothioate backbone modifications are indicated with an $^{\#}$. All other nucleotides are unmodified RNA. B oligonucleotides were constructed via ligation of B_1 and 5′-^{32}P labeled B_2 to incorporate ^{32}P into the backbone of B at the depicted location.

S7.2 RNase degradation and Dicer processing studies

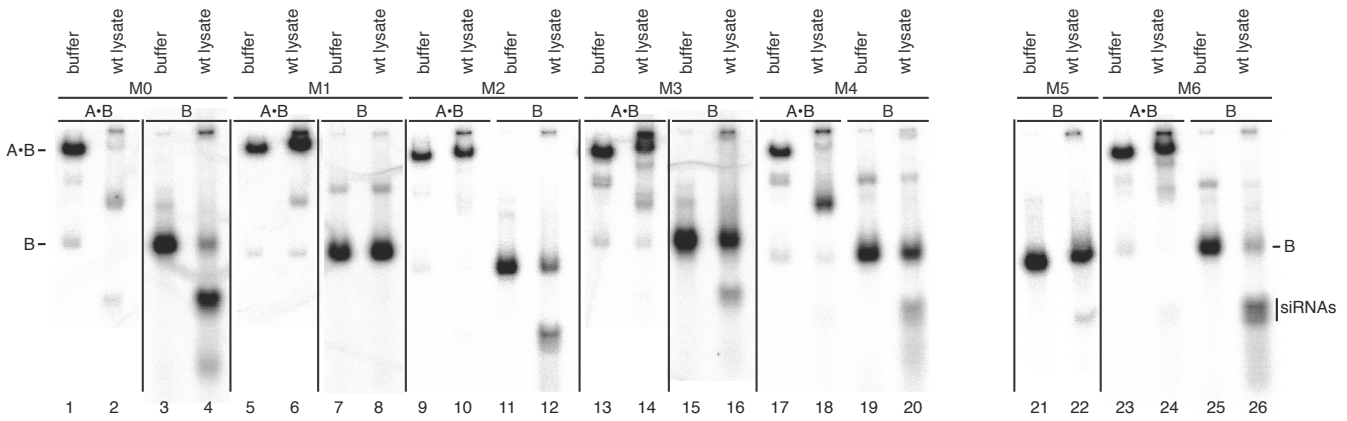

Figure S15: RNase degradation and Dicer processing of chemically modified shRNA B for the reverse mechanism (Y ⊣ X). Comparison of unmodified B (denoted M0) to six different chemical modifications (M1, ..., M6). Modifications to B must protect A·B from RNase degradation in lysate but still allow Dicer to cleave shRNA B into siRNAs. Experimental conditions: 2.5 nM A·B (A is 100% 2′OMe-RNA) or B were incubated in 1× Buffer D or 1.25 μg/μL wildtype lysate for 2 h at 37 °C and then separated by native PAGE. Gels from multiple experiments are displayed together for illustrative purposes (separated by vertical lines). Modifications M2 and M6 were the most successful, indicating that preventing nuclease activity at the 5′ and 3′ ends through 2′OMe-RNA modifications is a good strategy.

Modification	Description	scRNA A·B in lysate relative to buffer	shRNA B cleaved to siRNAs
M0	RNA (unmodified)	9%	81%
M1	2′OMe-RNA except 4 nt RNA at ligation site	233%	1%
M2	3 nt 2′OMe-RNA at 5′ and 3′ ends	118%	60%
M3	3 nt phosphorothioate backbone at 5′ and 3′ ends	94%	18%
M4	2′OMe-RNA loop (14 nt) plus alternating 2′OMe-RNA for siRNA sense strand (9 nt)	33%	37%
M5	2 nt DNA at 3′ end	–	6%
M6	1 nt 2′OMe-RNA at 5′ and 3′ ends	97%	83%

Table S6: RNase degradation and Dicer processing of chemically modified shRNA B for the reverse mechanism (Y ⊣ X). Protection from degradation is calculated as the percent A·B signal in lysate relative to buffer (background-subtracted A·B signal in lysate normalized by the background subtracted A·B signal in buffer). Complete protection from degradation would correspond to 100%. There is some variation due to well loading, but it is unclear why M1 A·B has significantly more signal in the lysate lane compared to the buffer lane. Dicer processing is calculated as the percent B processed into siRNAs in lysate (background-subtracted siRNA band normalized by the background-subtracted signal for the full lane). Complete Dicer processing of shRNA B would correspond to 100%. Modification M6 was determined to be the best modification to shRNA B due to the near complete protection of A·B from degradation while allowing >80% cleavage of shRNA B.

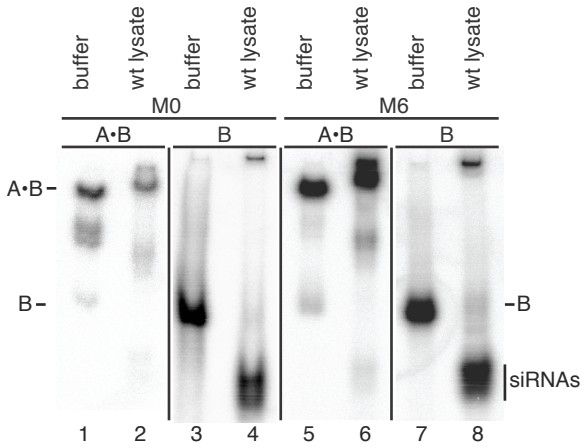

Figure S16: RNase degradation and Dicer processing of chemically modified shRNA B for the forward mechanism (X ⊣ Y). Modification M6 provides protection from degradation (lane 6) without impeding Dicer processing into siRNAs (lane 8). Experimental conditions: 2.5 nM A·B (A is 100% 2′OMe-RNA) or B were incubated in 1× Buffer D or 1.25 μg/μL wildtype lysate for 2 h at 37 °C and then separated by native PAGE. Gels from multiple experiments are displayed together for illustrative purposes (separated by vertical lines).

References

[1] Hochrein, L. M., Schwarzkopf, M., Shahgholi, M., Yin, P., and Pierce, N. A. (2013) Conditional Dicer substrate formation via shape and sequence transduction with small conditional RNAs. *J. Am. Chem. Soc.* 135, 17322–17330.

[2] Zadeh, J. N., Steenberg, C. D., Bois, J. S., Wolfe, B. R., Pierce, M. B., Khan, A. R., Dirks, R. M., and Pierce, N. A. (2011) NUPACK: Analysis and design of nucleic acid systems. *J. Comput. Chem.* 32, 170–173.

[3] Wolfe, B. R., Porubsky, N. J., Zadeh, J. N., Dirks, R. M., and Pierce, N. A. (2017) Constrained multistate sequence design for nucleic acid reaction pathway engineering. *J. Am. Chem. Soc.* 139, 3134–3144.

[4] Mathews, D. H., Sabina, J., Zuker, M., and Turner, D. H. (1999) Expanded sequence dependence of thermodynamic parameters improves prediction of RNA secondary structure. *J. Mol. Biol.* 288, 911–940.

[5] Sakurai, K., Amarzguioui, M., Kim, D. H., Alluin, J., Heale, B., Song, M. S., Gatignol, A., Behlke, M. A., and Rossi, J. J. (2011) A role for human Dicer in pre-RISC loading of siRNAs. *Nucleic Acids Res.* 39, 1510–1525.

[6] Pei, Y., Hancock, P. J., Zhang, H., Bartz, R., Cherrin, C., Innocent, N., Pomerantz, C. J., Seitzer, J., Koser, M. L., Abrams, M. T., Xu, Y., Kuklin, N. A., Burke, P. A., Sachs, A. B., Sepp-Lorenzino, L., and Barnett, S. F. (2010) Quantitative evaluation of siRNA delivery in vivo. *RNA* 16, 2553–2563.

[7] Roskams, J., Rodgers, L., and Mellick, A. S. (2002) *Lab Ref : a handbook of recipes, reagents, and other reference tools for use at the bench* (Cold Spring Harbor Laboratory Press, Cold Spring Harbor, NY).

[8] Gillen, C. M., and Forbush III, B. (1999) Functional interaction of the K-Cl cotransporter (KCC1) with the Na-K-Cl cotransporter in HEK-293 cells. *Am. J. Physiol. – Cell Physiol.* 276, C328–C336.

[9] Tuschl, T., Zamore, P. D., Lehmann, R., Bartel, D. P., and Sharp, P. A. (1999) Targeted mRNA degradation by double-stranded RNA in vitro. *Genes Dev.* 13, 3191–3197.

[10] Rouskin, S., Zubradt, M., Washietl, S., Kellis, M., and Weissman, J. S. (2014) Genome-wide probing of RNA structure reveals active unfolding of mRNA structures in vivo. *Nature* 505, 701–705.

[11] Sugimoto, N., Nakano, S., Katoh, M., Matsumura, A., Nakamuta, H., Ohmichi, T., Yoneyama, M., and Sasaki, M. (1995) Thermodynamic parameters to predict stability of RNA/DNA hybrid duplexes. *Biochemistry* 34, 11211–11216.

[12] Xia, T., SantaLucia, J., Jr, Burkard, M. E., Kierzek, R., Schroeder, S. J., Jiao, X., Cox, C., and Turner, D. H. (1998) Thermodynamic parameters for an expanded nearest-neighbor model for formation of RNA duplexes with Watson-Crick base pairs. *Biochemistry* 37, 14719–14735.

[13] Kierzek, E., Mathews, D. H., Ciesielska, A., Turner, D. H., and Kierzek, R. (2006) Nearest neighbor parameters for Watson-Crick complementary heteroduplexes formed between 2′-O-methyl RNA and RNA oligonucleotides. *Nucleic Acids Res.* 34, 3609–3614.

[14] Eastberg, J. H., Pelletier, J., and Stoddard, B. L. (2004) Recognition of DNA substrates by T4 bacteriophage polynucleotide kinase. *Nucleic Acids Res.* 32, 653–660.